

METHODOLOGY FOR THE DESIGN OF LNG TERMINALS IN A NEARSHORE ENVIRONMENT

Frédéric Jaouën

MARIN

P.O. Box 28, 6700 AA
Wageningen, The Netherlands
Email: f.jaouen@marin.nl

Olaf Waals

MARIN

P.O. Box 28, 6700 AA
Wageningen, The Netherlands
Email: o.waals@marin.nl

Martijn de Jong

Deltas

P.O. Box 177, 2600 MH
Delft, The Netherlands
Email: martijn.dejong@deltas.nl

Arne van der Hout

Deltas

P.O. Box 177, 2600 MH
Delft, The Netherlands
Email: arne.vanderhout@deltas.nl

Marios Christou

Imperial College London
London SW7 2AZ,

United Kingdom

Email: marios.christou@imperial.ac.uk

ABSTRACT

Nowadays, more and more nearshore LNG terminals are being built as it offers easy access to vessels coming from deep water and mitigates the risk by isolating regasification units from the cities. However, designing these terminals can be challenging in shallow water, as it is exposed to low-frequency waves which can excite the moored vessels at their natural periods. By lack of knowledge and adequate numerical simulation techniques, the effect of these low-frequency waves on the motions of moored vessels are unfortunately often ignored in the design. This is likely to result in an underestimation of the vessel motions and terminal downtime. In this paper, a methodology for the design of terminals in a nearshore wave climate is presented. The methodology consists of six steps which guide the engineer from the definition of the deep-water sea states to the calculation of the vessel motions and terminal downtime. In an initial stage, computational efficient tools are used, with the limitation that several approximations need to be made. In a later stage, more detailed but expensive methods are applied. The objective of this paper is to show how the developed methodology can give insight in the expected downtime due to the low-frequency waves in any nearshore mooring location. As an example, the methodology is applied on a fictive but realistic case, for which the motion response of a LNG carrier moored to a jetty on a sloping bottom is calculated. From seven years of deep-water sea states, the terminal downtime is estimated. The application of the methodology to the design case confirms that the terminal downtime can be significantly underestimated if shallow water effects are not taken into

account. So the influence of the water depth, bathymetry, wave directionality and low-frequency waves on the vessel motions should be investigated with care. However, the results obtained in the design case also show that the spectral shape of the low-frequency waves predicted by the wave models are sensitive to the tuning of numerical parameters. Tuning the wave models against model tests or full scale data is therefore highly recommended, because the motion response of a low-damped moored vessel can be dominated by the amount of low-frequency free wave energy at its natural periods.



Figure 1: Illustration of a nearshore terminal (source: www.projectconnect.com.au)

INTRODUCTION

Nowadays, more and more nearshore LNG terminals are being built as it mitigates the risk by isolating regasification units from the cities. Designing these terminals can be challenging in shallow water because it is exposed to infragravity waves ([1], [2], [3], [4]). As shown on Figure 2, infragravity waves are waves with periods between 30s and 300s, whereas wind waves have typical dominant periods between 1s and 25s. The infragravity waves are therefore likely to excite the vessel at the natural frequencies of the horizontal degrees of freedom, so it is important to take these waves into account for the operability assessment of the LNG terminal.

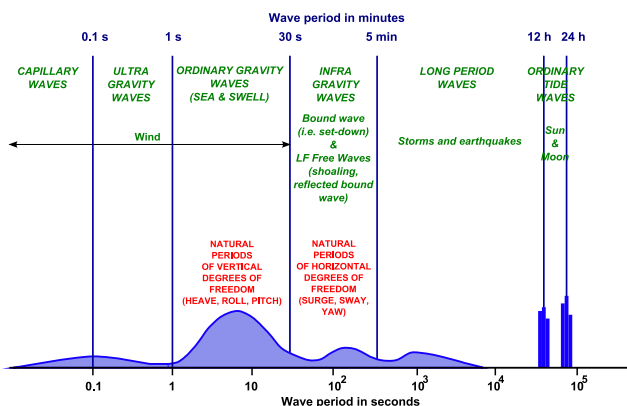


Figure 2: overview of typical wave periods

The different sources of infragravity waves are represented in Figure 3. The incoming infragravity waves consist both of the bound wave (also referred to as set-down [5]), which travels at the group velocity of the primary wave, and of the low-frequency (LF) free waves, which follow the dispersion relation. An incoming infragravity free wave can also be generated during the shoaling process of the primary wave. It is important to realize that the infragravity waves, which are long and low waves, do not become as steep as the wind waves when approaching the shoreline. So even if the incoming infragravity waves become larger when entering shallower water and can dissipate energy by wave breaking [6], a significant part of their energy can actually be reflected on the shoreline. This is also true for the bound wave, which is reflected as a low-frequency free wave. The infragravity wave field at the mooring location is therefore complex, originating from different sources, each having their own directions.

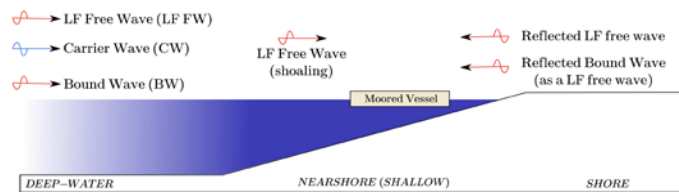


Figure 3: overview of all wave contributions

In order to gain knowledge on terminal design in shallow water, the Joint Industry Project (JIP) HAWAI was conducted from 2006 to 2008. Twenty-four companies participated in this JIP to investigate among other things the free and bound infragravity waves in the model test basin and in the field ([7]), the wave mechanics in shallow water, the drift forces in directional seas ([8],[9],[10]), the application of diffraction theory in shallow water ([11]), and the application of various wave models in intermediate water depths ([12]). This project greatly improved the insight in the behaviour of low-frequency shallow water waves and their interaction with offshore terminals. It was found for example that the motion response of vessels moored in shallow water can be dominated by the infragravity waves. The knowledge of nearshore wave development in combination with state of the art response models led to an increased understanding of vessel response in a wave basin ([7]). However, the step towards examining the effect of infragravity waves in a realistic environment was not made.

Based on the knowledge gained during the first project, the follow-up JIP HAWAII was conducted between 2009 and 2012 to investigate how the knowledge that was developed could be translated in a design methodology for an offshore terminal in a nearshore environment. The objective of the project was to develop a consistent design methodology for offshore terminals in a nearshore wave climate. In this paper the stepwise methodology developed within the JIP, as schematized in Figure 4, is presented and applied on a specific example. A detailed description of the methodology including recommendations is available in Annex B of this paper. It is noted that this paper focuses on the methodology itself, i.e. the results obtained from the design case are used as an illustration, but are not important in the absolute sense.

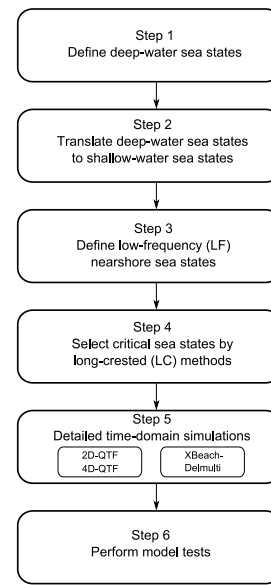


Figure 4: step-by-step design methodology

DESCRIPTION OF THE DESIGN METHODOLOGY

Step 1 : Define deep water sea states

The first step of the design methodology consists in determining the deep water sea states nearby the expected mooring location. The term deep-water refers to a regime in which the waves' properties are independent of the water depth. These offshore sea states can be obtained from hindcast data, satellite measurements or full scale buoy measurements. This data should include at least the significant wave height H_s , the wave peak period T_p and the mean wave direction MWD. It is recommended to obtain a set of data as complete as possible, including the full directional spectrum for both wind seas and swell. This is not always available though, and the spectral shape and directional spreading may need to be assumed if unknown. By running statistical tools on the data, the engineer can derive and analyze the deep water climate. The time traces of the original wave properties can for example be presented as scatter or quantile plots in order to check the consistency of the data prior to further processing. If consistent bias is found such as for example data gaps or outliers, the original data is compared to other sources of data and corrected if needed ([13]). The data correction consists for example in filling the gaps with interpolated or dummy values, or in removing data based on pre-set thresholds (e.g. when larger than 3 times the standard deviation). When this first step of the methodology is completed, one should have at his disposal a list with thousands of consistent and verified deep-water wave climates.

Application to the design case

For the purpose of the wave modelling, a fictitious island was set-up with surrounding water depth gradually increasing towards deep water ($>300m$). The fictitious island and water depths are presented in Figure 5 together with the assumed shallow water mooring location represented by a blue dot, and the deep water location represented by a red dot. The coordinate system used in the study case to define the direction of the environments and vessel heading is also shown in this figure. For the design case, the selected wave data at the deep water location is based on hindcast time-series of wave parameters for a period of 7 years ranging from 1997 to 2003 from the ECMWF (European Centre for Medium range Weather Forecast, see [14]) which runs operational atmospheric and wave forecasts. The data considered in this study is the analyzed values of the forecast, i.e. the 0-h forecast improved by means of data assimilation. The seven years of data lead to a total of 10,224 wave climates. Time traces of the significant wave height, peak period and mean wave directions in 6 hourly intervals were obtained as shown in Figure 6. This Figure shows that the significant wave height ranges from 1.0m to 3.5m for peak periods ranging from 8s to 25s. There is also a strong dominant mean wave propagation direction, which is a "coming-from" direction of about 180deg from the North in the compass coordinate system. This corresponds to a "going-to" direction of 90deg in the coordinate system shown in Figure 5.

Neither data gaps nor outliers were identified in the original data set, so the uncorrected data was used. The spectral shape and directional spreading of the deep water sea states were unfortunately not available, so the spectral shape of these sea states was assumed to follow the JONSWAP formulation with a peak enhancement factor $\gamma=3.3$. The directional spreading was assumed to follow the cos-m formulation as described in [15], with the m-parameter being 2 for the peak periods lower than 10s, and 7 otherwise. In practice, this means that the short-waves are more directionally spread than the long waves.

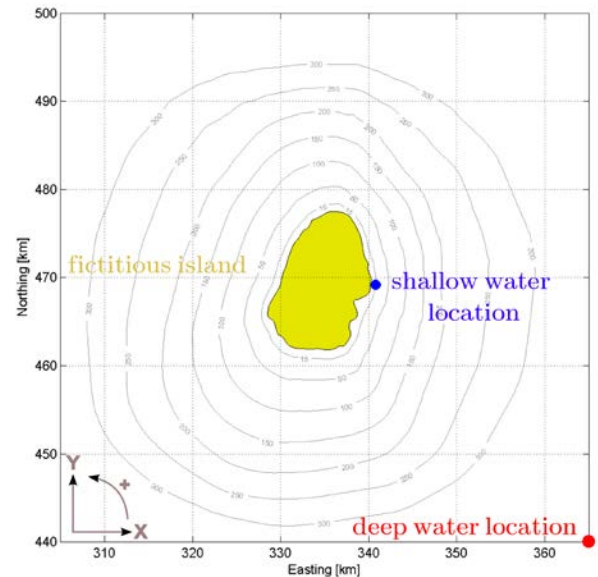


Figure 5: geometry of the fictitious island and surrounding bathymetry, with the deep and shallow water locations

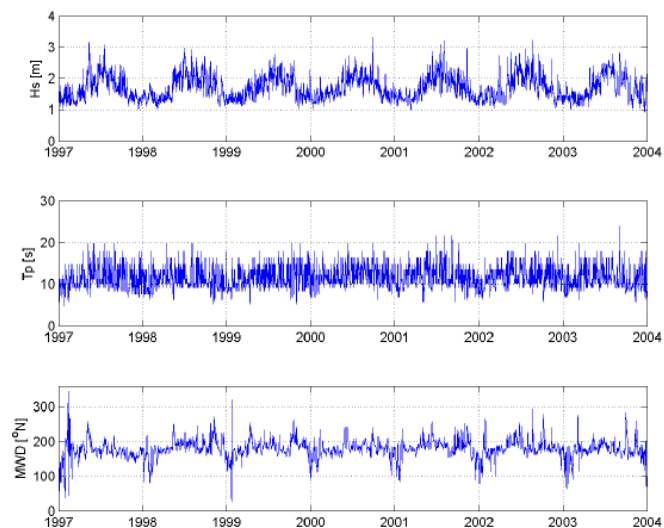


Figure 6: hindcast time series of the ECMWF wave parameters

Step 2 : Define primary nearshore sea states

The second step of the design methodology consists in transforming the deep-water primary sea states to nearshore primary sea states. The objective is to calculate the changes of the wave properties when the wave travels from the deep water to the shallow water mooring area. Deriving a wave climate in shallow-water is mostly based on transformation of deep-water wave data by means of wave modeling. The spectral wave model SWAN developed by Delft University of Technology can for example be used ([16]). The wave modeling can be carried out in stationary mode for predefined wave scenarios or alternatively in non-stationary mode by running the wave model for the whole multi-year data period. Although potentially more reliable, the latter method is often not feasible as it requires large computational efforts. The recommended methodology in transforming deep-water wave climates to a shallow-water location for a large amount of sea states is therefore to apply scenario-based wave modeling and climate transformation ([13]).

First, the SWAN model consisting of the considered bathymetry and boundary conditions is prepared. The boundary conditions describe the directional spectrum of the primary waves, the wind field, and eventually fields of water level and current at the boundaries of the computational domain. Then, the deep water wave climates are used to define a large series of so-called model scenarios. Typically, between 100 and 200 scenarios are selected, and consist of a combination of wind and wave combinations. The scenarios serve as input for the SWAN wave modeling and are considered as a mean representation of the offshore climate. The SWAN model is then applied to compute the wave conditions in the model domain for these scenarios, instead of thousands of wave climates as available in the multi-year wave data. The results consist of stationary fields of various wave parameters including H_s , T_p and MWD. Based on the results obtained for the selected scenarios, transformation matrices are made between the deep water wave properties and the shallow water wave properties. These matrices are then applied to transform the complete time series of deep-water wave parameters into time series of shallow-water wave parameters. By running the same statistical tool as for the deep-water wave climate, one can derive extreme statistics, joint-occurrence, persistence tables and wave roses at the shallow-water location. It is noted that the procedure also allows deriving wave climates at any other location in the model domain, without the need for redoing the time-consuming wave modeling.

Once this second step of the design methodology is completed, one should have a list of thousands of primary wave climates at the nearshore location.

Application to the design case

For the design case, 173 scenarios considered as a mean representation of the offshore climate were defined and calculated with SWAN. The bathymetry of the design case consists of a non-porous inclined bottom parallel to the

shoreline and with a slope 1:40 as shown on Figure 7. The mooring location is such that water depth is 15m at midship. The numerical grid used for the computations is 70km wide and 60km long and is represented in Figure 8.

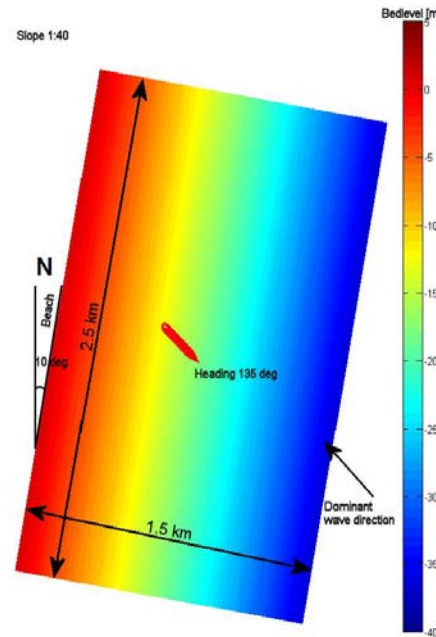


Figure 7: representation of the design case

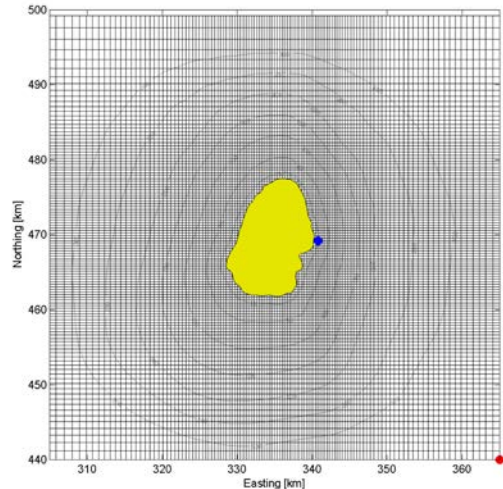


Figure 8: numerical grid for SWAN computations

An example of computed field of significant wave height and mean wave directions for one of the 173 scenarios is shown in Figure 9. The island is represented in blue color in the middle of the picture, where the significant wave height is zero. For this scenario, the deep-water wave properties are $H_s=1.63\text{m}$, $T_p=12.32\text{s}$, $\text{MWD}=90.63\text{deg}$ (towards North) and the spreading parameter m is assumed to be 7. Based on the results obtained with all scenarios, transformation matrices were calculated and

the complete time traces of deep-water wave properties were transformed to shallow water mooring location.

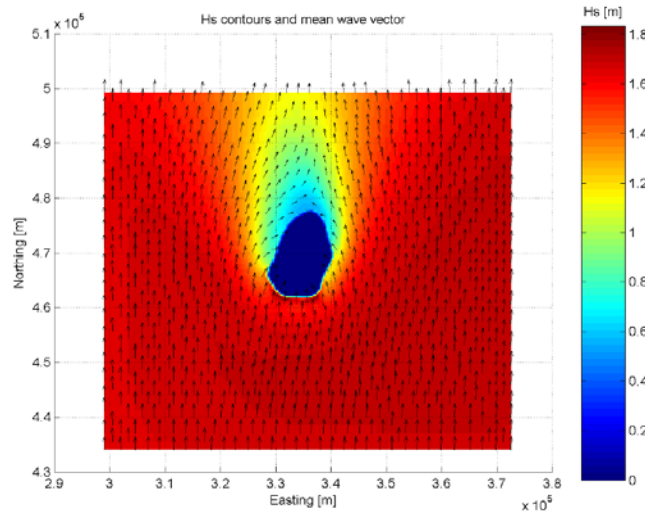


Figure 9: computed significant wave height and mean wave direction for one scenario

Figure 10 represents the wave rose plots both at the deep-water location and at the shallow-water mooring area. This Figure shows that there is a strong dominant wave direction at the mooring location. Most waves propagate with a direction 135deg. i.e. towards North-West. Based on the results of the wave transformation study as shown on this Figure, the heading of the moored vessel was selected to be 315deg, i.e. head-on in the primary waves to minimize the wave forces. The bow is therefore directed towards South-East, as illustrated in Figure 7.

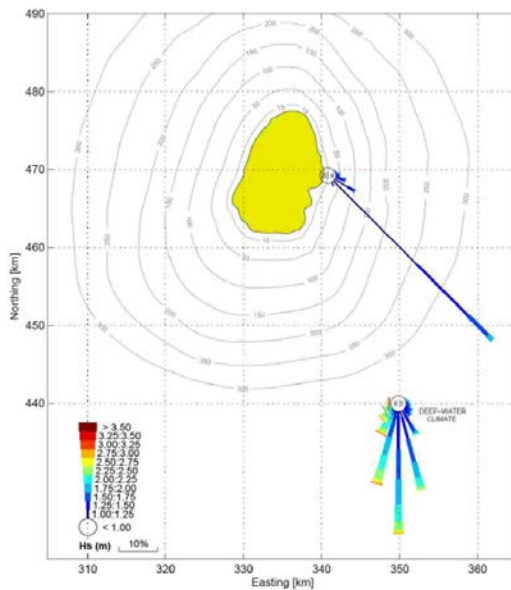


Figure 10: schematic indicating the fictitious island with surrounding bathymetry and the resulting transformation of the deep water climate to the nearshore using SWAN

Step 3 : Define low-frequency nearshore sea states

The third step of the methodology consists in determining the amount of infragravity waves (bound and free) at the mooring location for the multi-year wave data, such that their excitation forces on the moored vessel can be accounted for in the motion response calculation. This can be calculated by using empirical formulas as provided within the JIP HAWAI, frequency-domain wave models such as IDSB ([17]) or time-domain wave models such as XBeach ([18]) or SWASH ([19]). The advantages and drawbacks of these methods are summarized in Figure 11.

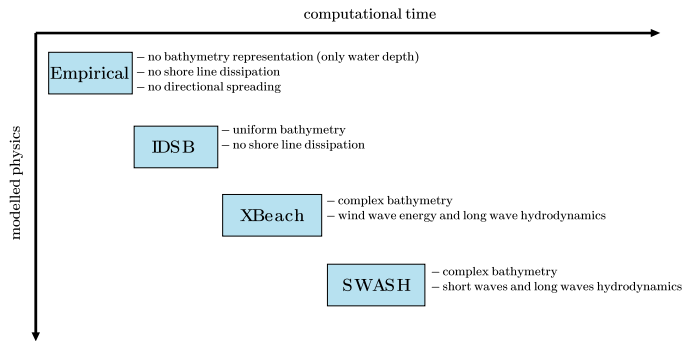


Figure 11: overview of available tools to calculate infragravity wave energy

On one hand, empirical formula are fast but provide neither the spectral shape nor the directions of the LF free waves, which therefore need to be assumed, that leads to inaccurate results. On the other hand, the time-domain wave models are more accurate, can consider a complex bathymetry, and calculate both the spectrum shape and directions, but are too time-consuming to calculate the complete multi-year wave climate. As a compromise, a frequency domain code as IDSB is found to be more suitable ([20], [21]). In IDSB, the spectral shape of the infragravity waves is calculated, but not the directions which need to be assumed to calculate their excitation on the moored vessel. When unknown, the directions can be assumed by considering that the infragravity free waves correspond to the reflected bound-wave, which is fully reflected against the straight shoreline. A consequence of this assumption is that all LF free waves are assumed to originate from the reflected bound wave, which means that the generation of incoming LF free waves during the shoaling of the primary waves is ignored. Based on an alongshore uniform bathymetry and directional spectra of the primary wave, IDSB calculates the total infragravity wave spectrum. By estimating the bound wave contribution using the equilibrium approach for a constant water depth, and subtracting it from the computed total infragravity wave spectrum, the LF free wave spectrum can be obtained. In the model, the incoming infragravity waves are only of the bound-type, i.e. the model does not include LF free waves from distant sources. The outgoing infragravity waves are free and can be leaky or trapped edge waves depending on the angle of incidence and bathymetry. It is important to note that the IDSB model requires calibration of the so-called breaking parameter

$\gamma = H_{max}/d$ and the friction coefficient c_f before it can be used. The breaking parameter places an upper limit to the maximum wave height as a function of the water depth and this significantly affects the wave height of the short waves, which in turn alters the magnitude of the infragravity waves. The friction coefficient only affects the infragravity waves. The friction coefficient employed in IDSB is not solely a physical parameter that represents the effects of sea bed friction on the waves, as it is also used to damp the infragravity waves to realistic magnitudes. This is required in IDSB, as damping is a nonlinear term which is not included in the model which is based on the linear infragravity wave equations. This damping is inherently included in more sophisticated models such as XBeach or SWASH. As such, it is not possible to pre-determine the friction coefficient from solely the physical properties of the sea bed, and calibration of the IDSB model is therefore a necessary step. The calibration of the frequency domain code can be done based on measurement data available in the literature for a similar bathymetry, or by running the more advanced and accurate time-domain tools for a limited number of cases.

Once this third step of the methodology is complete, one should have a list of thousands of primary wave climates, and infragravity free wave climates. The directions of both bound and free infragravity waves should also be known, whether they have been calculated or assumed.

Application to the design case

For the design case, the slope 1:40 was considered and the 10,224 nearshore wave climates as calculated by SWAN were prescribed at the boundary of the LF wave model domain depicted in red in Figure 12. The IDSB model was calibrated using the measurements of De Boers [22] for irregular waves propagating up an effective beach slope of 1 in 35.

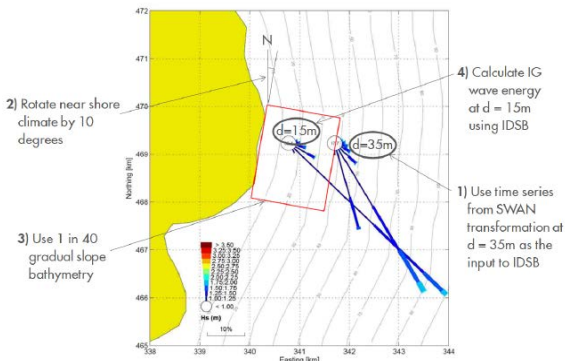


Figure 12: methodology for calculating the infragravity waves at 15m water depth with IDSB

As the multi-year data can be rapidly calculated with IDSB, sensitivity studies were also carried out to investigate the influence of the primary wave direction and directional spreading on the calculated infragravity waves. The computations are not only conducted for the “real” wave directions, for which the primary waves are travelling in the mean direction of propagation as calculated by the SWAN

simulations and shown in Figure 10. They are also conducted for the “perpendicular” directions, for which all of the incident primary waves are propagating perpendicular to the shoreline. The computations were also repeated for various directional spreadings varying from long-crested (LC) waves ($m=1000$) to short-crested waves ($m=30$). Lower values of m , although more consistent with the assumptions made in step 1, could not be modelled in IDSB. The results of the computations are presented in Figure 13 through Figure 16, which represent the histogram distributions of the total infragravity wave energy as a percentage of the primary wave energy and the proportion of free to total infragravity wave energy. Table 1 summarizes the results by presenting the most probable values from the histograms.

The difference in the distributions for the two scenarios given in blue and red in the figures show that the mean direction of propagation of the primary waves has a significant influence on the results. For the “real” direction, there is a wide distribution for the proportion of total infragravity waves to primary waves, with the infragravity wave energy ranging between 0% and 11% of the primary waves. This distribution is a lot narrower for the “perpendicular” scenario, as in this case there is no variation due to the mean direction of propagation and the main parameters are the significant wave height, the peak period and the directional spreading of the primary waves. In contrast, the “real direction” scenario introduces the mean direction of propagation as an extra variable, and this leads to a broad-banded histogram distribution. The similarity of the band-width of the two distributions in Figure 14 and Figure 16 indicates that the mean direction of propagation only plays a small role in determining the proportion of free to total infragravity wave energy.

Consulting Table 1 and considering the most realistic scenario for the design case, which corresponds to $m = 30$ with the “real” mean direction of propagation, we can note that the proportion of the infragravity waves to primary wave energy is approximately 5% and the free infragravity waves form 80% of the total IG wave energy, with a corresponding significant wave height of 5cm. However, it must be emphasized that the distributions produced by these numerical simulations are fairly broad-banded and it is necessary to consider the correct mean direction of propagation as well as directional spreading parameter. Therefore, the results obtained on this design case cannot be generalized so there is clearly a need to perform numerical simulations for each specific situation.

Table 1: summary of the results corresponding to the most probable value from the histograms

m	Direction CW	IG/Primary Hs [%]	Free/Total IG Hs [%]	Free IG wave Hs [cm]
1000	Perpendicular	7.0	75	5.5
1000	Real	6.0	75	6.5
100	Perpendicular	7.0	80	6.2
100	Real	5.0	80	5.7
30	Perpendicular	7.5	85	6.5
30	Real	5.0	80	5.0

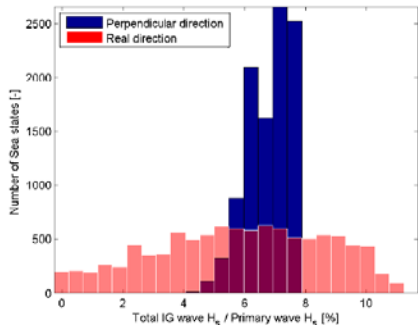


Figure 13: distribution of the percentage of IG wave energy to the carrier wave energy for $m=1000$ (LC)

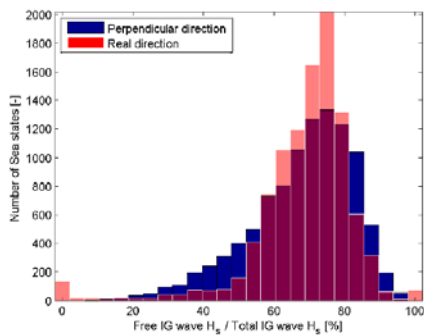


Figure 14: distribution of the percentage of free IG wave energy to the total IG wave energy for $m=1000$ (LC)

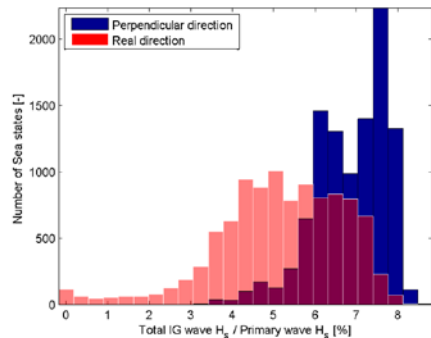


Figure 15: distribution of the percentage of IG wave energy to the carrier wave energy for $m=30$

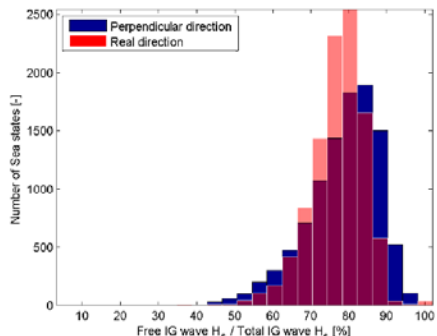


Figure 16: distribution of the percentage of free IG wave energy to the total IG wave energy for $m=30$

Step 4 : Select critical sea states

The fourth step of the design methodology consists in screening the thousands of sea states describing the nearshore wave climate to obtain a limited number of relevant design cases. Screening the multi-year climate is a necessary step because the highest offshore wave conditions do not necessarily lead to the most critical wave conditions at the mooring site. The methods used should be reasonably accurate, but they should be especially fast to be able to assess the downtime for the multi-year wave data within a couple of days. This is achieved by neglecting wave directionality and by approximating the bathymetry by a flat bottom locally for the calculation of added mass, potential damping and wave forces. Because these calculations can be performed relatively fast, it is practical to conduct extensive sensitivity studies at this stage. For example, the sensitivity of the downtime to the LF free waves can be assessed by comparing the results obtained with and without LF free waves. This will indicate whether these waves are worth being taken into account for the design, or whether the traditional deep-water engineering approach ignoring the LF free waves can be followed. Because detailed calculations and model tests may be carried out later for the selected environments, it is crucial to select the most relevant cases.

The motion response of the moored vessel exposed to primary waves (inc. set-down), and eventually LF free waves, is calculated by resolving the equation of motion for all nearshore sea states. For the primary sea states, the second order wave forces are also considered using the five contributions of the Quadratic Transfer Function (QTF) as formulated by Pinkster [23]. This can be done in the frequency domain for systems which can be assumed linear for small excursions such as a soft-yoke, or in the time-domain for non-linear systems such as a jetty mooring. Based on the calculated vessel response, the downtime can be estimated by choosing one or several criteria which need to be fulfilled by the system in order to be able to operate. Typically, these criteria relate to the maximum mooring line loads, motions or accelerations experienced by the vessel. The comparison of the downtime using plots similar to Figure 17 is an easy way to quantify the influence of the LF free waves, but also the influence of other physical parameters such as the bathymetry, the water depth, the seed and other environments such as current and wind.

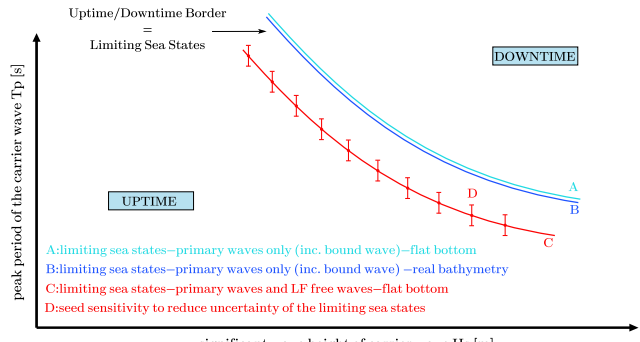


Figure 17: steps used in the screening method

First, the influence of the flat bottom approximation needs to be investigated. A flat bottom locally at the mooring location is assumed in this step of the methodology for robustness and time-efficiency. Using the average water depth under the vessel as equivalent water depth should be a reasonable approximation in most cases. However, a flat bottom is not representative of the reality, so it is important to verify the suitability of the selected equivalent water depth. This is done by verifying that the flat bottom approach is conservative compared to the real bathymetry, i.e. the downtime obtained with the equivalent flat bottom should not be lower than the downtime obtained with the real bathymetry. For that purpose, the motion response of the vessel should be calculated for all primary waves both for the flat bottom and for the real bathymetry. For the real bathymetry, the shoaling of the carrier wave on the wave forces, added mass and potential damping is taken into account by diffracting panels on the sea bottom ([24], [25]). The downtime and limiting sea states as depicted should be found relatively similar for both configurations, as depicted on Figure 17 for cases (A) and (B).

Then, the influence of the low-frequency waves can be assessed using the equivalent flat bottom configuration. Similarly to the primary waves, the LF free waves are also assumed to be long-crested in this step of the methodology. If the phase of the LF free wave with respect to the primary wave is not known, a spectral formulation without phases (frequency domain) or with random phases (time-domain) can be used for computational efficiency. The direction of the LF free waves need to be assumed as well if unknown, which can be done by assuming that the LF free waves correspond to the reflected bound wave. The influence of the LF free waves on the motion response of the vessel can be quantified by comparing the downtime and limiting sea states obtained with and without LF free waves, i.e. by comparing the cases (A) and (C) in Figure 17. Typically, for a very mild slope and deeper water, the energy of the LF free waves should be limited and thus their influence on the design as well. For other cases, the LF free waves may actually dominate the vessel response.

Finally, it is important to systematically perform a random seed sensitivity study, in order to make conclusions on seed-converged solutions. The influence of the seed (i.e. randomly distributed phase of the primary wave spectrum) on the vessel motions can be large due to the relatively small amount of low-frequency vessel oscillations within a 3h wave climate. However, performing a seed sensitivity study on the whole data set may be very time consuming and not feasible in practice. It is therefore recommended to perform a seed sensitivity study for the cases which are close to the downtime/uptime border, in order to reduce the uncertainty band between uptime and downtime climates. In a standard frequency domain, the seed converged solution is automatically calculated because no phase information is included. In time-domain, this can be done by increasing the simulation time, or by performing three-hour simulations for many seeds. A small part of the simulations (e.g.

10) using different seeds (e.g. 10 seeds) can be run to assess the variability due to different realizations of the wave climates. At the end of this step, one should have determined a flat bottom water depth equivalent to the real bathymetry, and have estimated accurately the border downtime-uptime with and without LF free waves. If the LF free waves are found not to affect significantly the downtime, they can be ignored and the methodology can be aborted. Otherwise, typically between 15 and 30 cases which are close to the uptime-downtime border, i.e. at the limit of the criterion exceedance, can be selected to be investigated in more detail in the next steps of the methodology.

Application to the design case

For the application of the methodology to the design case, the motion response of a LNG carrier moored to a jetty was calculated. The main particulars of the considered vessel and the panel distribution used to calculate the hydrodynamic database are summarized in Annex A. The jetty mooring consists of sixteen identical lines and four cell fenders. The calculation was done in the time domain because a jetty mooring is a non-linear system. The MARIN software aNySIM is used to perform the time-domain calculations. This program can simulate the coupled motion behavior of multiple floating and non-floating bodies including effects such as mooring systems and hydrodynamic interactions, and has been regularly used for similar studies ([26], [27]). It integrates the equation of motion taking into account the self inertia, added inertia, wave loads, damping loads and restoring forces. For the design case, the external forces consist of the first and second order forces due to the primary wave, the first order forces due to the LF free waves, and the forces applied by the berthing lines and fenders. The criterion that was used to define the downtime was the mooring line load that should not exceed 744kN. Extensive sensitivity studies have been conducted by varying the water depth and the bathymetry. The influence of the LF free waves as calculated by the empirical formulae and by IDSB has been investigated as well. For these numerical studies, the simplified and academic approach illustrated on Figure 18 has been followed by considering that the shoreline is perpendicular to the main wave direction. The approach corresponding to the “real directions is illustrated on Figure 19.

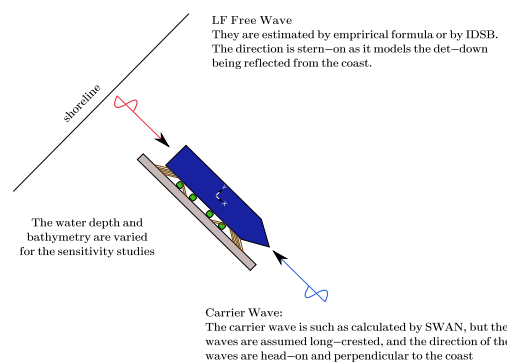


Figure 18: setup corresponding to the “perpendicular” directions, and used for the sensitivity studies

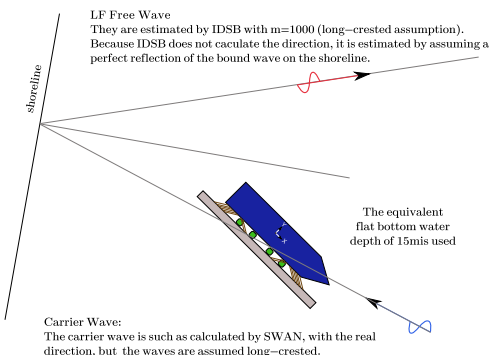


Figure 19: setup corresponding to the “real” directions and corresponding to the design case

The direction of the LF free waves was assumed to correspond to the reflected bound wave as it is not calculated with these approaches. The spectrum shape of the LF free waves is calculated by IDSB, but not by the empirical formula, for which a white noise spectrum ranging from 30s to 200s was assumed. The downtime calculated for the different investigated cases are summarized in Table 2. Based on this Table, the following observations can be made:

- The downtime obtained for a flat bottom configuration with constant water depth 21.25m is slightly larger than the one obtained using a sloping bottom with water depth at midship 21.25m. This confirms that approximating a sloping bottom with the average water depth under the vessel is a conservative assumption.
- The downtime obtained in primary waves for both the “real” and “perpendicular” directions are very similar. This is because the primary waves have a strong dominant direction as shown on Figure 10.
- The downtime increases from 3.2% to 3.4% when the LF free waves as predicted by IDSB are taken into account, and increases up to 5.1% when the LF free waves energy is predicted by the empirical formulae. This shows not only that the downtime increases in the presence of LF free waves, but also that the downtime assessment is very sensitive to the method used to calculate the LF free waves.
- The downtime decreases drastically when water depth increases. Increasing the water depth from 15m to 17m basically divides the downtime by a factor 2.7.

Table 2: summary of the screening calculation results

Water Depth [m]	Bathymetry	Primary Waves	Low-Frequency Free Waves	Downtime
15.00	Flat	Real	—	3.10%
15.00	Flat	Perpendicular	—	3.20%
17.00	Flat	Perpendicular	—	1.20%
21.25	Flat	Perpendicular	—	0.22%
30.00	Flat	Perpendicular	—	0.05%
21.25	Slope	Perpendicular	—	0.06%
15.00	Flat	Perpendicular	Empirical	5.10%
15.00	Flat	Perpendicular	IDSB (m=1000)	3.40%

Figure 20 illustrates the results obtained in primary waves for the “perpendicular” direction and for a water depth of 15m. The uptimes sea states are represented by grey markers whereas the downtime sea states are represented with black markers. The downtime obtained for this case amounts 3.20%, which means that the maximum allowable mooring line load has been exceeded in 327 of the 10,224 environments. As an illustration of the design methodology, 17 cases represented by green markers on Figure 20 have been selected for further investigation in the next steps of the methodology. It is noted that the Hs and Tp which have been selected are fairly spread, i.e. they are not all close to the uptime/downtime border. This has been done to apply the last step of the methodology on diverse combinations of Hs and Tp, and also because it was not known in advance how much would the uptime/downtime border be shifted when applying the detailed methods.

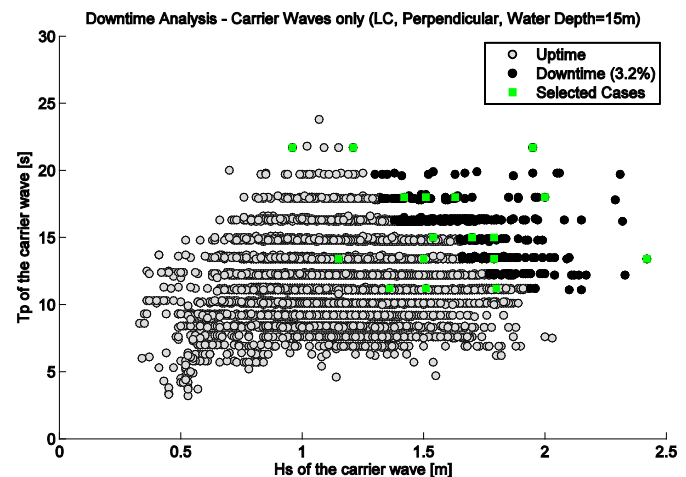


Figure 20: visualization of downtime for one case

Based on the application of the methodology to the design case, it can be noted that the downtime rate is very dependent on the water depth. Furthermore, the downtime increases when LF free waves are taken into account. However, the LF free waves as predicted by the empirical method and by the frequency domain code IDSB led to very different downtime estimates. This is mainly because the spectrum of the LF free waves differ for both methods. Because the spectrum shape and especially the amount of energy at the natural period of the vessel dominates the vessel response, the empirical methods is not recommended within the methodology to obtain accurate results.

Step 5: Perform detailed time-domain calculations

In the previous section, a few cases have been selected among the thousands cases available in the multi-year wave data. This selection was based on long-crested simulations and estimates of the LF wave spectra based on frequency-domain LF wave models. In reality, the wave climate is likely not to be long-crested and it is important to estimate the effect of the wave directionality on the design. Therefore, more detailed time-domain calculations are performed, taking the wave directionality of both the primary waves and the LF free waves into account.

An overview of the methods that can be used to calculate the motion response of the moored vessel is given in Table 3. Method A was used in the previous step of the methodology. Methods B, C and D account for directionality of the waves and form the focus of this section. For these three methods, the first-order forces due to the primary waves are calculated using the hydrodynamic database and considering the direction of each wave component. These methods only differ in the way the infragravity waves (bound and free) are accounted for.

Table 3: summary of the methods that can be used

	Method A	Method B	Method C	Method D
Accuracy	*	**	***	****
Primary Waves	SWAN	SWAN	SWAN	SWAN
Primary Wave Forces (1 st order)	FRAO	FRAO	FRAO	FRAO
Primary Wave Forces (2 nd order)	2D QTF I–IV (LC)	2D QTF I–IV (directional spreading)	4D QTF I–IV (directional spreading + dir. interaction)	2D QTF I–IV (directional spreading)
IG Waves	IDSB (IG free only)	IDSB (IG free only)	IDSB (IG free only)	XBeach (bound + free)
IG Free Wave Forces	FRAO	FRAO	FRAO	Coupling XBeach + Diffraction
IG Bound Wave Force	2D–QTF–V (LC)	2D–QTF–V (directional spreading)	4D–QTF–V (directional spreading + directional interactions)	
Vessel Motions	Time Domain Code	Time Domain Code	Time Domain Code	Time Domain Code

For methods B and C, the drift forces in directional seas are calculated using the 2D-QTF or the more advanced 4D-QTF as described in [10]. With the 2D-QTF approach, the second order wave forces due to the primary waves are calculated using 2D-QTF, which means that only wave components travelling in the same direction interact and contribute to the drift force. With the 4D-QTF approach, wave components travelling in different directions also interact and contribute to the slow-varying drift forces. The drawback of these methods is that both the direction and the directional spreading of the LF free waves need to be assumed as this is not calculated by IDSB. A consequence of this assumption is that all LF free waves are assumed to originate from the reflected bound wave, which means that the

generation of incoming LF free waves during the shoaling of the primary waves is ignored.

For this reason, the more advanced method D is introduced, which consists of a coupling between a time-domain LF wave model and a diffraction code to calculate the forces due to the LF waves. The coupling approach is illustrated in Figure 21. The XBeach wave model calculates the total infragravity wave (bound and free) at the vessel location (but without the ship being actually present), which are converted into time traces of vessel forces by a diffraction code. This wave model includes a detailed description of the bathymetry, even for the most complex ones involving channels, breakwaters, or non-uniform coastlines. The wave model simulates the influence of the bathymetry on the infragravity waves, and therefore accounts for the LF free wave generated during shoaling, which is not the case in IDSB. Furthermore, the directions and directional spreading of the LF free waves do not need to be assumed anymore as it is automatically included in the wave model results. It is noted that because the bound wave is automatically included in the wave model results, the second-order wave forces due to the primary waves are calculated with QTF contributions I through IV only, as formulated by Pinkster in [23]. The contribution V, which accounts for the set-down effect on the low-frequency wave forces, is excluded.

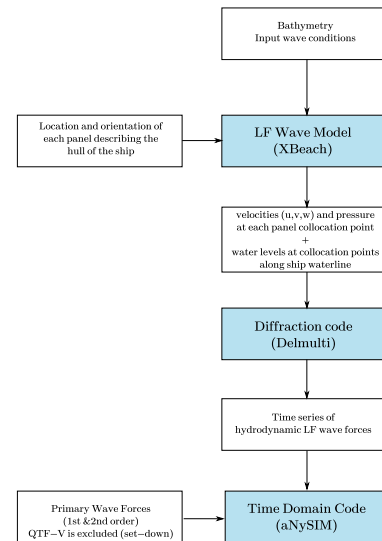


Figure 21: schematic overview of the coupling model chain

Finally, a simplified coupling can also be used as an alternative to the advanced coupling method described above. This simplified approach ignores the diffraction and considers that the LF wave forces are dominated by the so-called Froude-Krylov forces. These forces correspond to the summation of the forces on the vessel hull resulting from the undisturbed infragravity wave field. The results obtained with this simplified coupling are not presented in this paper, but are shown to be quite promising though in [28].

Application to the design case

For the application of the methodology to the design case, the motion response of the vessel was calculated in the time-domain using aNySIM. The forces on the vessel, resulting vessel motions and mooring line loads are computed with the four methods shown in Table 3 for the 17 selected cases. To illustrate the effect of directionality and of the LF free waves, the calculations were conducted with and without LF free waves. For the coupling method, the wave model XBeach and the diffraction code DELMULTI [29] were used. Figure 22 is a snapshot of XBeach output for one of the cases. The arrows illustrate typical directions of incoming and reflected infragravity waves in the nearshore region. The red shape represents the ship moored nearshore in a water depth of 15m. The colors represent the surface elevation of the total infragravity wave field including bound and free waves. The short waves are not shown on this figure.

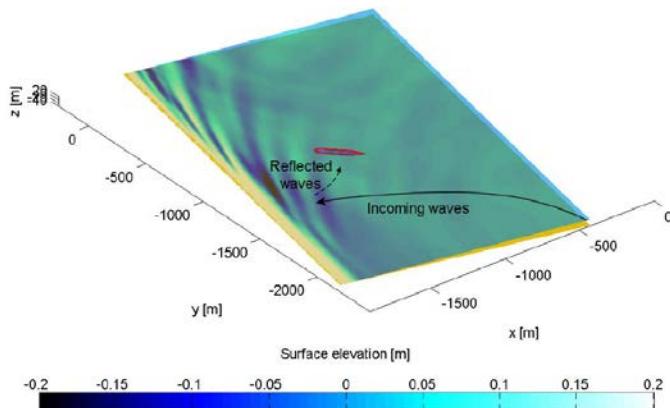


Figure 22: snapshot of the LF wave field computed by XBeach for one sea state

The results of the motion response calculations for the 17 selected cases can be visualized in Figure 23. The colored dots in the figures represent standard deviations of surge, for that combination of primary wave height H_s and wave period T_p . A black circle around a colored dot indicates that the downtime criterion is exceeded for that wave condition according to the applied method. By comparing the results obtained with and without LF free waves, we can conclude that the effect of the LF free waves on the results is relatively small for the investigated case, because differences are hardly visible between the plots located on the left side (no LF free waves) and on the right side (with LF free waves). The reason is that the LF free wave energy predicted by IDSB is not located in the vicinity of the natural periods of the vessel, which are 76s and 81s for surge and sway respectively. Therefore, the LF free waves predicted by IDSB do not excite the vessel at its natural frequency. The influence of the wave directionality is much larger, and the vessel response predicted with 4D-QTF seems slightly larger than with 2D-QTF. It is noted that the results obtained with the XBeach-Delmulti coupling approach are

closer to the 2D-QTF approach than to the 4D-QTF approach. This is expected because the 2D-QTF was used for the coupling approach, instead of the more accurate 4D-QTF as it was not possible to exclude the contribution V from the QTF with the 4D-QTF approach at the time the study was conducted. In other words, the drift forces due to the contributions QTF I-IV are the same for the 2D-QTF approach and for the XBeach-Delmulti coupling approach.

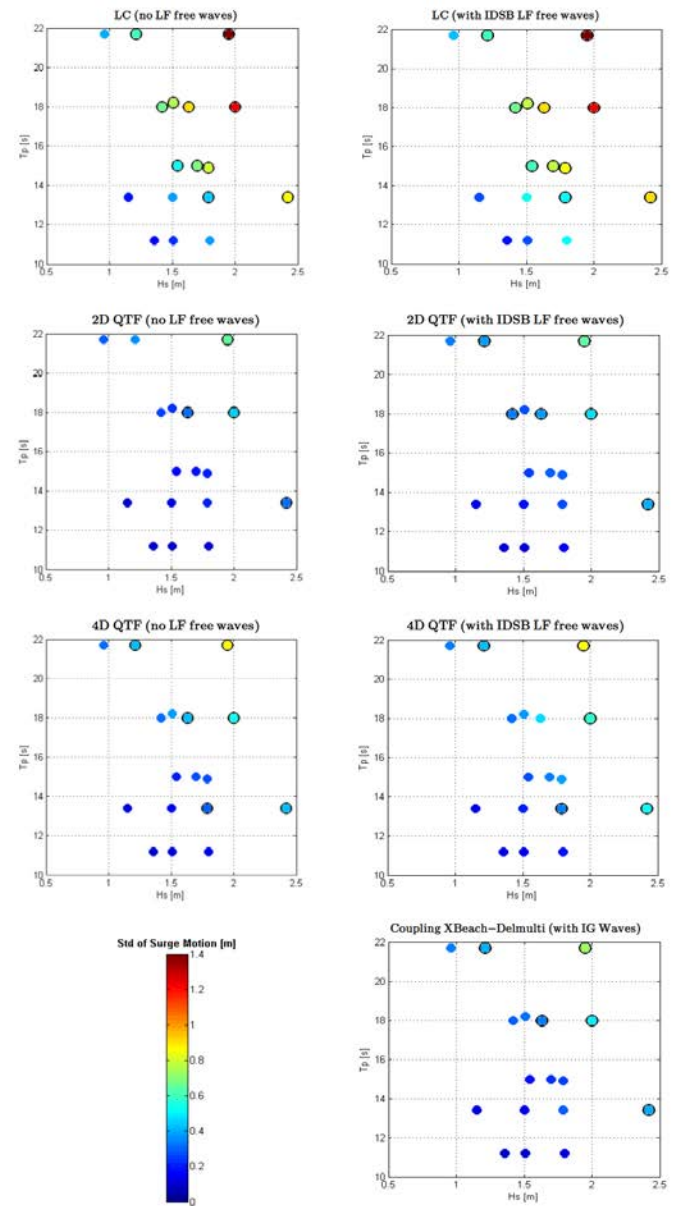


Figure 23: standard deviation of surge motions in primary waves with and without LF free waves for different methods

Step 6 : Perform model test campaign

In the previous sections, a numerical model has been built and the motion response of the vessel has been calculated with numerical methods of increasing complexity. The calculations were performed with long-crested as well as short-crested waves and showed the influence of the low-frequency free waves and bathymetry/coastline on the motion response of the vessel. As a final step, it is recommended to carry out a model test campaign on the moored vessel. This is a costly approach compared to numerical simulations, but necessary to verify the numerical model. The model test results should confirm that the numerical methods can predict the spectrum of infragravity waves accurately, which is crucial to predict the low-frequency motion response of the vessel correctly. The results of the model tests can be used to obtain the final response of the vessel by using the lessons learned from the JIP HAWAII [7], and to verify and validate the numerical studies performed in steps 1 to 5 of the methodology presented herein.

CONCLUSIONS

The design of LNG terminals is challenging as infragravity waves can excite the moored vessels at their natural frequencies. In this paper, a methodology is presented to design terminals in shallow water and account for the influence of the infragravity waves on the motion response of vessels and analyze the downtime. State of the art methods with increasing complexity are applied all along the stepwise methodology to predict the response of the moored vessel at a specific mooring location, in a combination of primary waves and low-frequency free waves. The relevance of the LF free waves for the considered design can also be assessed at different stages of the methodology, such that one can evaluate whether the methodology can be aborted.

The presented methodology and application on a specific design case shows that the Joint Industry Project HAWAII was successful in developing a consistent design methodology which gathers the knowledge of the nearshore wave models and state of the art vessel response models. However, the results obtained on the design case also indicate that estimating the infragravity directional wave spectrum at the mooring location is the critical step of the methodology. Both empirical formulae and LF wave models have been used, which have shown significant differences in the amount of energy as well as in the spectral shape. Furthermore, the directions of the LF free waves are not always calculated and may need to be roughly assumed. The consequences on the motion response of the moored vessel can be large as the amount of energy located at the natural period of the vessel dominates its motion response. Therefore, the tuning of the LF wave models used to predict the amount of infragravity wave energy is a critical step, and basin model tests or full scale measurements at the mooring location are recommended to obtain valuable data for the validation of the wave models. The amount of wave energy could be verified,

and preferably an array of wave probes could be installed to obtain the directions or main directional spreading.

FUTURE WORK

In this paper, the advanced computations using the coupling between the wave model XBeach and the time-domain response model have been conducted using the 2D-QTF approach, ignoring the interactions between wave components traveling in different directions. In the future, the 17 cases should be recalculated using the 4D-QTF approach. Furthermore, a number of key steps of the methodology should be validated by comparing the numerical results published in this paper to model test data.

ACKNOWLEDGMENTS

The calculations presented in this paper were performed as part of the HAWAII JIP, a Joint Industry Project aiming at developing a methodology for the design of LNG terminals in a nearshore environment. The authors would like to express their gratitude to the HAWAII participants for their financial contributions and their input and feedback during the progress meetings. The authors would also like to thank Dr. Jo Pinkster for his contribution and advice in the coupling between the wave model XBeach and the diffraction code DELMULTI.

REFERENCES

- [1] Elgar et al., (1992), "Observations of Infragravity Waves", *Journal of Geophysical Research*, Vol. 97, No. C10, Pages 15, 573-15,577.
- [2] Herbers, T.H.C. et al., (1994) "Infragravity-frequency motions on the shelf. Part I: forced waves", *Journal of Physical Oceanography*, 24, 917-927
- [3] Herbers, T.H.C. et al., (1995), "Infragravity-frequency (0.005-0.05Hz) motions on the shelf. Part II: free waves", *Journal of Physical Oceanography*, 25, 1063-1079.
- [4] Thompson, J., (2006), "Infragravity Waves over Topography: Generation, Dissipation and Reflection", *PhD Thesis*.
- [5] Longuet-Higgins, M.S. and Stewart, R.W., (1964) "Radiation stresses in water waves; a physical discussion, with applications", *Deep Sea Research*, Vol. 11.
- [6] Van Dongeren, A. et al., (2007), "Shoaling and shoreline dissipation of low-frequency waves", *Journal of Geophysical Research*, Vol. 112.

- [7] Waals, O.J., (2009), "On the Application of Advanced Wave Analysis in Shallow Water Model Testing (Wave Splitting)", *OMAE2009-79413*.
- [8] Renaud M. et al., (2008), "Second order wave loads on a LNG Carrier in Multi Directional Waves", *OMAE2008-57409*.
- [9] Pinkster J.A., (2009), "Wave Drift Forces in Directional Seas in Shallow Water", *OMAE2009-80110*.
- [10] Waals, O.J., (2009), "The Effect of Wave Directionality on Low Frequency Motions and Mooring Forces", *OMAE2009-79412*.
- [11] Naciri M. and Sergent E., (2009), "Diffraction / Radiation Study of 135,000M3 Storage Capacity LNG Carrier in Shallow Water – A Benchmark Study", *OMAE2009-79645*.
- [12] De Jong, M.P.C. et al., (2009), "Calculation of low-frequency waves in shallow water and comparison to common practice in diffraction methods", *OMAE2009-79401*.
- [13] Van Os, J.J.A.M. and Caires, S., (2011), "How to carry out metocean studies", *OMAE2011-49066*.
- [14] Dee, D.P. et al., (2011), "The ERA-Interim reanalysis: configuration and performance of the data assimilation system", *Journal of the Royal Meteorological Society, Volume 137, Issue 656, pages 553-597*.
- [15] Hennig, J. et al., (2015), "Shortcrest: Directional Wave Measurements at MARIN", *OMAE2015-41169*.
- [16] Booij, N. et al., (1999), "A third-generation wave model for coastal regions, Part I, Model description and validation", *J. Geoph. Res., 104(C4), 7649-7666*.
- [17] Reniers, A.J.H.M. et al., (2002), "Linear modeling of infragravity waves during Delilah", *J. Geophys. Res., 107(C10), 3137, doi:10.1029/2001JC001083*.
- [18] Roelvink, D., et al., (2009), "Modelling storm impacts on beaches, dunes and barrier islands", *Coastal Engineering, Volume 56, Issues 11-12, November-December 2009, Pages 1133-1152*.
- [19] Zijlema, M. et al., (2011), "SWASH: An operational public domain code for simulating wave fields and rapidly varied flows in coastal waters", *Coastal Engineering, Volume 58, Issue 10, October 2011, Pages 992-1012*.
- [20] Christou M. et al., (2011), "Analysis of shallow water wave measurements recorded at the Field Research Facility", *Proceedings of the 12th International Workshop on Wave Hindcasting & Forecasting & 3rd Coastal Hazards Symposium*
- [21] Reniers, A.J.H.M. et al., (2010), "Estimation of infragravity waves at intermediate water depth", *Coastal Engineering 57, pp. 52-61*.
- [22] De Boers, M., "Simulation of a surf zone with a barred beach , report 1 – wave heights and wave breaking" *Communications on Hydraulic and Geotechnical Engineering: TUD Technical University Delft*
- [23] Pinkster J.A., (1980), "Low Frequency Second Order Wave Exciting Forces on Floating Structures", *Phd. Thesis.*
- [24] Buchner, B., (2006), "The motions of a ship on a sloped seabed", *OMAE 2006-92321*.
- [25] Pinkster, J.A., (2011), "A multi-domain approach in 3D diffraction calculations", *OMAE2011-49480*.
- [26] Naciri, M. et al., (2007), "Time-domain simulations of side-by-side moored vessels – Lessons learnt from a benchmark test", *OMAE2007-29756*.
- [27] De Wilde, J.J. et al., (2009), "Direct Time Domain Downtime Assessment for LNG Operations using Computer Cluster", *ISOPE 2009*.
- [28] Van der Hout, A. et al., (2015), "Long waves in intermediate depths and their influence on the design of nearshore terminals", *IAHR 2015*.
- [29] Pinkster, J.A., "The influence of a free surface on passing ship effects", *International shipbuilding progress, 51(4), 313-338*.

ANNEX A

Table 4: properties of the LNG carrier

Designation	Symbol	Unit	Value
Length between perpendiculars	Lpp	[m]	274.0
Breadth	B	[m]	44.2
Draft	T	[m]	11.0
Water depth at midship	WD	[m]	15.000
Displacement	Δ	[m ³]	97,120
Mass	M	[ton]	99,548
Roll radius of gyration	K _{xx}	[m]	15.2
Pitch radius of gyration	K _{yy}	[m]	68.5
Yaw radius of gyration	K _{zz}	[m]	68.5
Transverse metacentre	K _{Mt}	[m]	21.07
Longitudinal metacentre	K _{Ml}	[m]	482.2
Number of panels		—	1,102
Position of CoG in X	LCG	[m]	-1.06
Position of CoG in X	KG	[m]	16.3

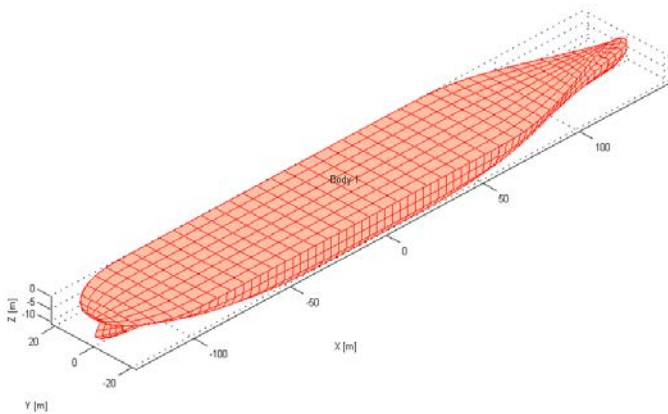
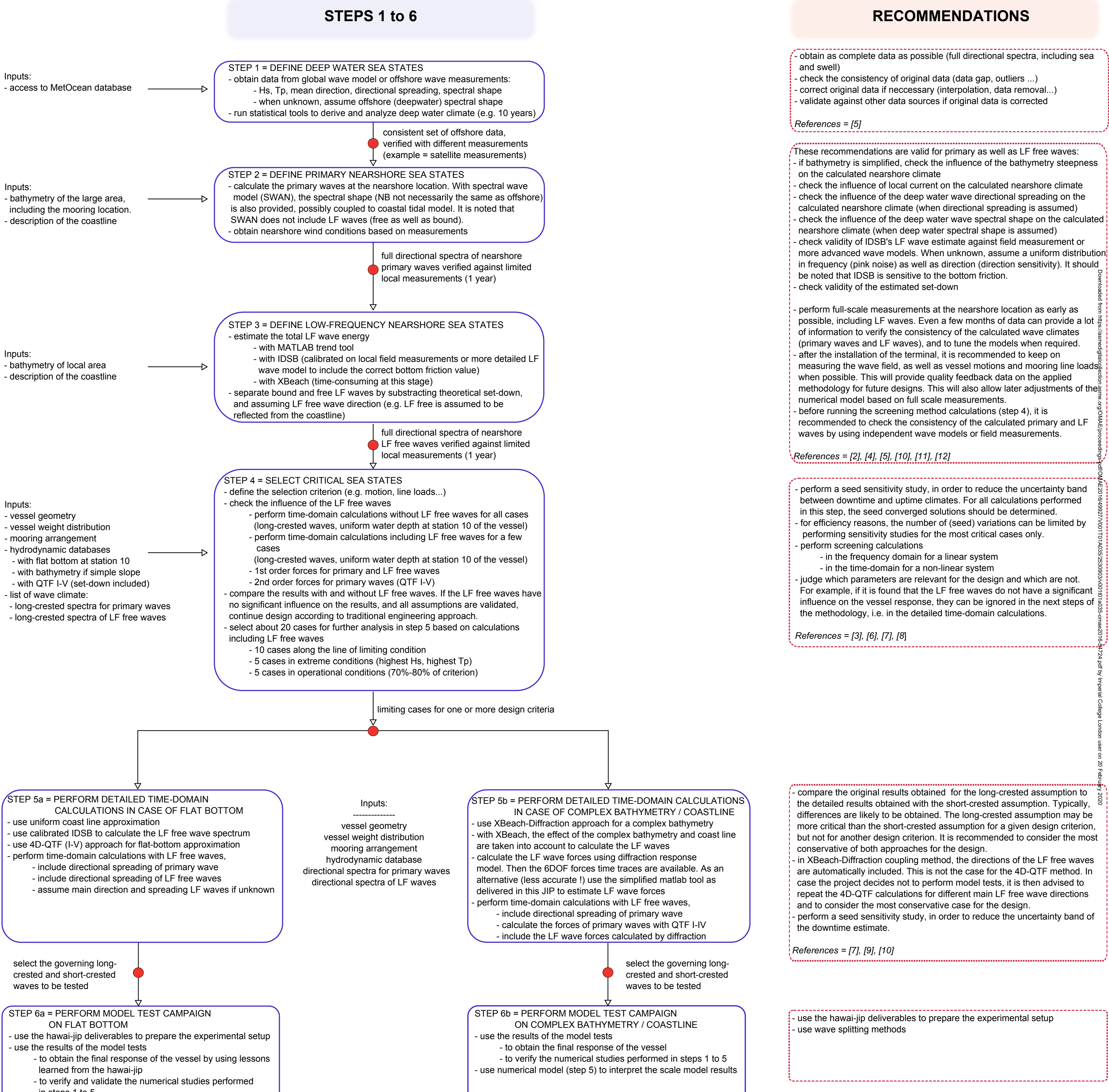


Figure 24: panel distribution of the LNGC

METHODOLOGY FOR THE DESIGN OF LNG TERMINALS IN A NEARSHORE ENVIRONMENT

HAWAII-JIP



REPORTS:

- [1] HAWAII-JIP Project Plan. version 2.0.
- [2] Christou, M. (Shell). IDSB calculation of the low-frequency wave energy. HAWAII-JIP Report 2012.
- [3] de Hauteclercq, G. (BV). Local bathymetry effects on seakeeping. HAWAII-JIP Report 2012.
- [4] de Jong, M. Phase coupling between primary waves and bound low-frequency waves. HAWAII-JIP Report 2012.
- [5] Graaff, de.R.F (Deltaires). Neashore wave transformation. HAWAII-JIP Report 2010.
- [6] Jaouen, F., Otto, W. (MARIN). Frequency Domain Computations of a LNGC Motion response Spectra. HAWAII-JIP Report 2012.
- [7] Jaouen, F. (MARIN). Time Domain Calculations of a LNGC Motion Response. HAWAII-JIP Report 2012.
- [8] Pinkster, J.A. (PMH). Computation of the behavior of a LNG carrier on a sloping bottom. HAWAII-JIP Report 2011.
- [9] van der Hout, A. (Deltaires) Description of a coupling from XBeach to a diffraction method. HAWAII-JIP Report 2012.
- [10] van der Hout, A. (Deltaires) Detailed nearshore LF wave modelling - results of the case study. HAWAII-JIP Report 2012.
- [11] van Essen, S. (TU-Delft/Deltaires) Directional Spectrum Analysis of Low Frequency Waves. MSC Thesis 2012.
- [12] van Thiel de Vries, J. (Deltaires). Evaluation of XBeach as forcing model for ship motions. HAWAII-JIP Report 2012.

SOFTWARE:

- ANYSIM: time-domain simulation software (MARIN)
- DELMULTI: diffraction code (PMH)
- DIFFRAC: diffraction code (MARIN)
- IDSB: frequency-domain LF wave model (developed by Reniers 2002, also used by Shell)
- MATLAB script to calculate motion response in frequency domain (MARIN)
- MATLAB script to estimate amount of LF waves (Deltaires)
- MATLAB script to calculate Morison forces / Froude-Krylov forces (Deltaires)
- SWAN: wave model for simulation of waves from deep to shallow water (Deltaires)
- XBEACH: open source time-domain LF wave model. (Deltaires)